

A Servo-Controlled Capacitive Pressure Sensor Using a Capped-Cylinder Structure Microfabricated by a Three-Mask Process

Jae-Sung Park and Yogesh B. Gianchandani, *Member, IEEE*

Abstract—A silicon-micromachined servo-controlled capacitive pressure sensor is described. The use of a capped-cylinder shape with pick-off electrodes external to a sealed cavity permits this device to be fabricated in only three masking steps. Device behavior is evaluated experimentally and by finite element analysis. A fabricated device with 2 mm diameter, 9.7 μm structural thickness and 10 μm cavity height provides a measured sensitivity of 0.516 V/kPa over a dynamic range of 20–100 kPa gauge pressure, with a nonlinearity of <3.22% of full scale. The open-loop sensitivity of this device averaged over a dynamic range of 0–250 kPa is -408 ppm/kPa. A voltage bias applied to the servo-electrode can be used to tune both the open-loop and servo-controlled sensitivity by more than 30%. An alternative design in which the Si electrode is segmented to relieve residual stress provides 10–20% more open-loop sensitivity with similar structural dimensions. Fabricated devices are sealed within a metal package filled with an inert dielectric liquid. This enhanced open-loop sensitivity by a factor of about 1.7, and in servo-controlled operation, reduced restoring voltage by a similar factor. Measurements and analysis of temperature responses of these devices are presented. [861]

Index Terms—Dissolved wafer process, liquid encapsulation, pressure sensor, servo-controller.

I. INTRODUCTION

MICROMACHINED capacitive pressure sensors generally operate by sensing the downward displacement of a thin, flexible diaphragm using an electrode located beneath it [1], [2]. They tend to provide higher sensitivity, lower temperature coefficients, and lower power consumption than piezoresistive pressure sensors, which sense the deformation of a diaphragm by changes in stress at various locations on its surface. For these benefits, capacitive pressure sensors tend to compromise linearity and/or dynamic range.

Servo-controlled operation of a sensor can potentially improve the dynamic range and linearity, and also help in other ways. A few servo-controlled pressure sensors have been reported in recent years [3], [4]. Typically, the pressure-induced deflection of the diaphragm is balanced by an opposing electrostatic force. Although this is a natural choice when a capacitive

pick-off already exists in the device, it faces two constraints. The first is that applied voltages provide only attractive forces. This adds design and fabrication complexity because another actuation electrode must be located above the diaphragm. Past efforts have used double-sided wafer processing or as many as 15 masking steps—including device encapsulation, which is a significant asset—to accomplish this. The second constraint is that for voltages smaller than the pull-in voltage (at which the diaphragm collapses to the actuating electrode), the electrostatic pressure is smaller than the external pressure. To compensate for this, the servo-actuation electrode must be larger than the flexible diaphragm [4].

Although the area constraint cannot be easily circumvented, the fabrication complexity of a servo-controlled pressure sensor can be simplified using an unconventional device structure. This paper reports on the servo-controlled operation of a pressure sensor fabricated by a 3-mask process¹ using p^{++} Si as the structural material and glass as the substrate. The structure is similar to an open-loop pressure sensor reported in [5], [6]. As illustrated in Fig. 1, this device includes a sealed cavity formed between the substrate and a diaphragm that extends outward to form a deformable skirt or flap. The sidewall serves as a flexural hinge about which the diaphragm and skirt may flex. In open-loop operation, as the external pressure increases, the center of the diaphragm is deflected *downward* while the skirt is deflected *upward*. This movement is sensed capacitively by an electrode located underneath the skirt. The location of the sense electrode eliminates the need for lead transfer from inside the sealed cavity. More importantly, for servo-controlled operation, it permits the deflection of the skirt to be balanced by a voltage bias on the sense electrode. A separate actuation electrode located above the diaphragm is unnecessary. Moreover, the concentric layout of the sealed cavity and the skirt permits the electrode to naturally occupy a larger area than the diaphragm, as preferred for electrostatic feedback. A point of distinction from other implementations is that in this feedback scheme the skirt, and not necessarily the diaphragm, is restored to its reference position. The resulting performance is evaluated in the following sections.

The device is sealed within a metal package which has a flexible diaphragm. An inert liquid ambient is used within the package to transmit the pressure to the sensors. The dielectric liquid also serves to enhance the sensitivity of the pickoff. In servo-controlled operation, the higher dielectric constant of

Manuscript received May 7, 2002; revised November 6, 2002. Subject Editor G. Stemme.

J.-S. Park was with the Department of Mechanical Engineering University of Wisconsin, Madison WI 53706 USA. He is now with Shriner's Hospital, Boston, MA USA

Y. B. Gianchandani was with the Departments of Mechanical Engineering and Electrical and Computer Engineering, University of Wisconsin, Madison WI 53706 USA. He is now with the Electrical and Computer Science Department, University of Michigan, Ann Arbor, MI 48109-2122 USA (yogesh@umich.edu).

Digital Object Identifier 10.1109/JMEMS.2003.809953

¹Portions of this manuscript have appeared in conference abstract form in [7].

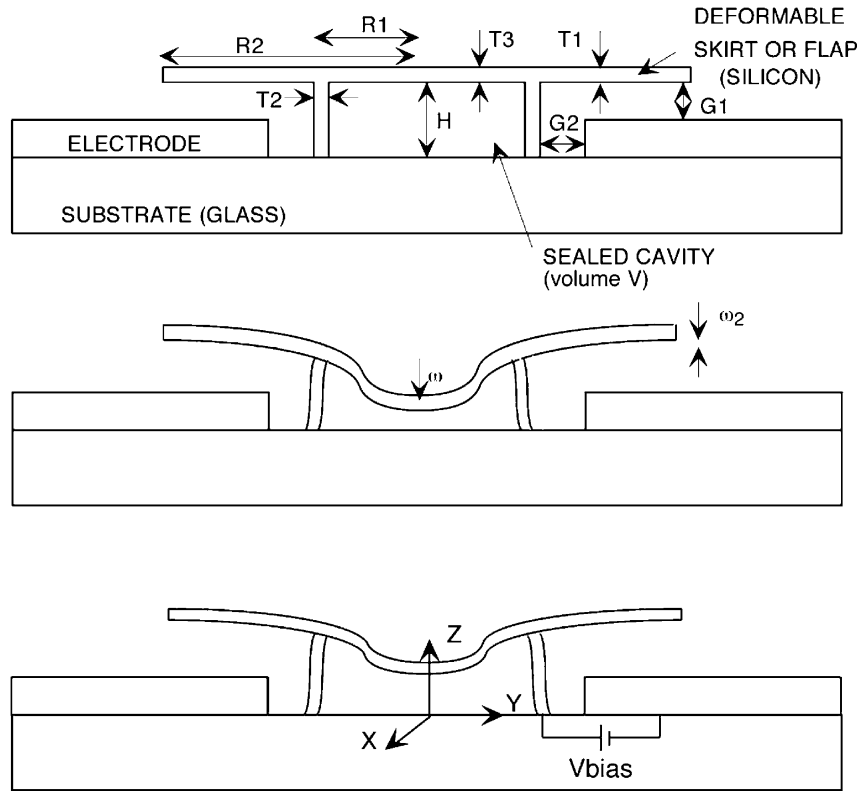


Fig. 1. Electrostatic attraction between the electrode and skirt opposes the deflection due to external pressure.

the medium also helps to reduce the operating voltage. In this paper, new results in modeling, fabrication and packaging, and experimental measurements of the sealed capacitive pressure sensor are described in Sections II, III, and IV, respectively. The open-loop performance is compared to servo-controlled behavior. The impact of packaging and temperature responses are assessed. Theoretical estimation of damping noise in a liquid environment is provided.

II. DEVICE STRUCTURE AND MODELING

A. Governing Equations

The deflection of the sensing diaphragm depends on its structural dimensions and the pressure across it. Depending on the magnitude of this deflection, the mathematical model and FEA model both vary. When deflection of the plate is larger than a half of its thickness, it is treated as a large deflection, for which stretching of the diaphragm should be considered in addition to its bending [8]. Since most sealed pressure sensors are sealed in vacuum to prevent the temperature dependence that would be caused by expansion of trapped gas, the diaphragm deflection at atmospheric pressure is significant and large deflection approximation is needed. This is true especially when the diaphragm is thin. The general governing differential equation for deflection of a thin plate is expressed as [8]

$$\frac{\partial^4 w}{\partial x^4} + 2\frac{\partial^4 w}{\partial x^2 \partial y^2} + \frac{\partial^4 w}{\partial y^4} = \frac{t}{D} \left[\frac{P}{t} + \frac{\partial^2 \phi}{\partial y^2} \frac{\partial^2 w}{\partial x^2} + \frac{\partial^2 \phi}{\partial x^2} \frac{\partial^2 w}{\partial y^2} - 2\frac{\partial^2 \phi}{\partial x \partial y} \frac{\partial^2 w}{\partial x \partial y} \right] \quad (1)$$

where P , w , t , D and ϕ are pressure, mid-plane displacement, plate thickness, plane flexural rigidity, and stress function, respectively. The exact solution for this equation exists only for very few cases [8]. However, when the deflection is small, the last three terms in (1) can be dropped and it is easier to handle.

Another device component which is critical to performance is the cylindrical sidewall. As pressure is applied to the sensor, the sidewall bends inward. This behavior can be described by [8], [9]:

$$\frac{d^4 r}{dz^4} + 4\beta^4 r = \frac{P}{D}; \quad \beta = \sqrt[4]{\frac{Et}{4R^2 D}} = \sqrt[4]{\frac{3(1-\nu^2)}{R^2 t^2}} \quad (2)$$

where r , P , E , t , R and ν are inward displacement, pressure, Young's modulus, thickness of the cylinder, radius of the cylinder and Poisson's ratio, respectively. The sum of particular and homogeneous solutions of the equation is

$$r_p(z) + r_h(z) = e^{-\beta z}(C_1 \cos \beta z + C_2 \sin \beta z) + e^{\beta z}(C_3 \cos \beta z + C_4 \sin \beta z) + f(z) \quad (3)$$

where $f(z)$ is the particular solution which depends on specific loads. For the devices mentioned in this paper, βz is much less than π (the case for short cylinders), and this means the load to the footprint of the cylindrical sidewall affects device behavior significantly [8], [9]. For example, the initial strain at the device footprint can affect device performance by changing the slope of the sidewall and stress state of the skirt electrode. These characteristics can affect the temperature coefficient of offset (TCO) and temperature coefficient of sensitivity (TCS).

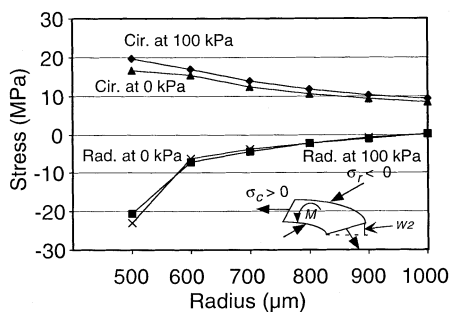


Fig. 2. ANSYS results for circumferential and radial stresses for 0 kPa and 100 kPa for the device with dimensions $T1 = T3 = 12 \mu\text{m}$, $T2 = 20 \mu\text{m}$, $H = G1 = 15 \mu\text{m}$, $R1 = 500 \mu\text{m}$, and $R2 = 1000 \mu\text{m}$. The residual stress from bonding at 450°C and 15 MPa tensile stress from boron doping are considered. A displacement, $w2$, of the skirt electrode, serves as a moment arm which combines with the tensile circumferential stress and compressive radial stress to create a bending moment.

The last device component is the skirt electrode, which moves upward and inward when pressure is applied to the diaphragm. This component can be also described by (1).

Since the analytical model must solve the equations above simultaneously, it is more convenient to use finite element analysis (FEA). The open-loop response for this pressure sensor was calculated by ANSYS using element Solid 95 for the structural material and Contac 49 for the sealed cavity.

B. Segmented Skirt Electrode

When pressure is applied to the diaphragm, the sidewall deflects inward, while the skirt electrode deflects upwards forming a conical shape. Resistance to this deflection comes not only from the stiffness of the sidewall, but also from the skirt electrode, which is under tensile circumferential stress and compressive radial stress that result from the nature of the fabrication process and design of the device. However, the stiffness contribution from the skirt reduces as its deflection increases. Finite element analysis was performed for a structure with dimensions $T1 = T3 = 12 \mu\text{m}$, $T2 = 20 \mu\text{m}$, $H = G1 = 15 \mu\text{m}$, $R1 = 500 \mu\text{m}$, and $R2 = 1000 \mu\text{m}$, with the residual stress from bonding at 450°C and 15 MPa intrinsic tensile stress, which will be explained later. Results show that in open-loop operation, as the applied pressure increases from 0 kPa to 100 kPa, the tensile circumferential stress decreases from 19.6 MPa to 16.6 MPa, while the compressive radial stress at the inner perimeter of the skirt increases from -20.4 MPa to -22.9 MPa . Thus, as pressure increases, the circumferential and radial stresses change from the initial residual stress, albeit not very much (see Fig. 2). Under applied pressure the skirt electrode deflects upward, increasing the moment arm for the stress in the skirt electrode. Since the stresses are relatively constant while the moment arm increases, the total bending moment on the skirt electrode increases, causing additional deflection at elevated pressures.

An alternative design, which has a radially segmented skirt electrode, is also evaluated. Eight 45° segments are formed from each skirt. This device is almost free of radial and circumferential stresses and provides more deflection by reducing the stiffness of the skirt electrode.

The responses of both devices to differential pressure were calculated assuming that there was no initial deflection. The di-

mensions of the devices were $T1 = T3 = 12 \mu\text{m}$, $T2 = 15 \mu\text{m}$, $R1 = 500 \mu\text{m}$, $R2 = 1000 \mu\text{m}$, $H = G1 = 15 \mu\text{m}$. It was assumed that the Si structure was bonded to the glass substrate at 450°C . At 25°C , pressure upto 100 kPa was simulated across the diaphragm. (In the case of a sealed cavity, this would be the difference between the applied pressure and the cavity pressure.) The device with the segmented electrode showed a sensitivity (defined as $\Delta C/C/\Delta P$, the fractional change in capacitance per unit change in pressure) of -113 ppm/kPa , while the device with a continuous electrode showed -103 ppm/kPa . Thus, the former provides $\sim 10\%$ higher sensitivity.

C. Device Height and Capacitance

As the height of the sidewall increases, so does the deflection of the skirt electrode at any given pressure. This can potentially increase sensitivity. However, the capacitance is inversely proportional to the average distance between the skirt and the thin film electrode patterned on the substrate. To understand the relation between the device height and sensitivity, FEA was performed. The simulated pressure was less than 100 kPa to eliminate the need for large deflection analysis. The dimensions used were $T1 = T3 = 12 \mu\text{m}$, $T2 = 15 \mu\text{m}$, $H = G1 = 15 \mu\text{m}$, $R1 = 500 \mu\text{m}$, and $R2 = 1000 \mu\text{m}$. For this set of dimensions, the absolute value of the sensitivity decreases as the height increases as reported previously [5], [6]. It was also noted in [5], [6] that one way to get higher sensitivity is to make $G1$ smaller than H . This can be done by using a thicker electrode metal or partially countersinking the structure into the substrate. Setting dimensional variables, $T1 = T2 = T3 = 5 \mu\text{m}$, $R = 500 \mu\text{m}$, $R2 = 1000 \mu\text{m}$, $H = 30 \mu\text{m}$, and $G1 = 5 \mu\text{m}$, large deflection simulations indicated that the open-loop sensitivity was -2900 ppm/kPa when the diaphragm was not in contact with the substrate, i.e., in nontouch mode, and -270 ppm/kPa in touch mode.

D. Sidewall and Diaphragm Thickness

The sensitivity of the device with the continuous (unsegmented) skirt electrode was calculated at different values of sidewall thickness ($T2$) and diaphragm thickness ($T1 = T3$). The device height was fixed at $15 \mu\text{m}$ and the applied pressure on the diaphragm was in the range of 0–100 kPa across the diaphragm. The resulting sensitivity map is shown in Fig. 3. As the sidewall thickness ($T2$) decreases, its stiffness decreases, and the sensitivity increases regardless of the diaphragm thickness. In addition, the sensitivity shows a maximum at a certain diaphragm thickness, because very thick diaphragms do not deflect adequately, and very thin diaphragms cannot provide sufficient force to bend the sidewall. For a $25\text{-}\mu\text{m}$ -thick sidewall, the sensitivity is maximum for a $15\text{-}\mu\text{m}$ -thick diaphragm, whereas for a $15\text{-}\mu\text{m}$ -thick sidewall, the sensitivity is maximum for an $8\text{-}\mu\text{m}$ -thick diaphragm. The overall trend favors a thinner sidewall.

E. Residual Stress

Another critical parameter for the device behavior is residual stress in the pressure sensor. It affects not only the device sensitivity, but also the initial state of the pressure sensor. The residual

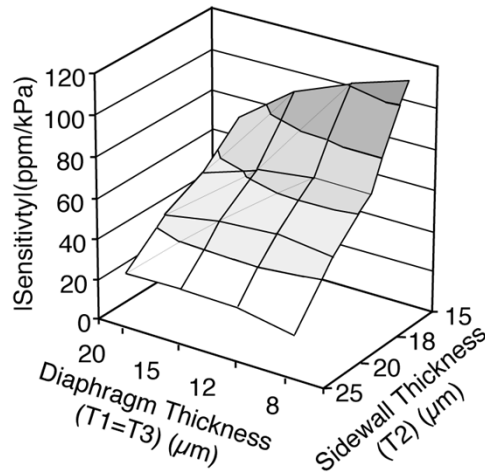


Fig. 3. Sensitivity for the device with continuous skirt electrode. It is assumed that $H = 15 \mu\text{m}$, $R1 = 500 \mu\text{m}$, $R2 = 1000 \mu\text{m}$, and $G1 = 15 \mu\text{m}$, and pressure range is 0–100 kPa.

stress in the dissolved wafer process comes from thermal expansion mismatch between Si structural material and glass substrate accumulated between $\approx 450^\circ\text{C}$, the temperature at which they are bonded together, and the operating temperature. It also has a component from boron doping, which is about 15 MPa intrinsic tensile [9]–[11]. These stress components were included in all FEA analysis described in this paper.

In order to evaluate device behavior over a wide temperature range, the coefficient of thermal expansion (CTE) of Si and glass must be evaluated as a function of temperature. A piece-wise linear approximation with seven values of the relative CTE of Si with respect to glass (Corning Pyrex #7740) is taken in the range of 0–550 °C to approximate true nonlinear expansion [12]. The average relative CTE for the purpose of calculating bonding stress is

$$(\alpha_{\text{relative}})_{\text{avg}} = \frac{\int_{T_0}^T \alpha_{\text{relative}}(T) dT}{T - T_0};$$

$$\alpha_{\text{relative}}(T) = \alpha_{\text{Si}}(T) - \alpha_{\text{glass}}(T) \quad (4)$$

where α is CTE, T is temperature of operation, and T_0 is bonding temperature. These averaged values are provided to ANSYS at the specified temperatures of concern, and the device strain state at the specified temperature changes can be calculated.

After bonding in the range of 300–500 °C, the center diaphragm is under tensile stress. This is reflected in the skirt electrode as a radial compressive stress, which varies with temperature. (Note that elevated bonding temperatures in the vicinity of 550 °C result in compressive residual stress for the diaphragm with undesirable consequences [14].) For comparison, the temperature dependent residual strains for the device with a continuous skirt electrode and with a segmented skirt electrode were calculated. The capacitance responses for devices with $T1 = T3 = 12 \mu\text{m}$, $T2 = 25 \mu\text{m}$, $R1 = 500 \mu\text{m}$, $R2 = 1000 \mu\text{m}$, $H = G1 = 15 \mu\text{m}$ at zero pressure across the diaphragm are shown in Fig. 4. It was assumed that the bonding temperature was 450 °C, leading to 18 MPa tensile residual stress.

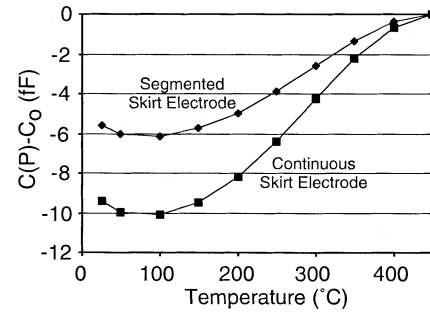


Fig. 4. Capacitance responses to temperature change for the device with $T1 = T3 = 12 \mu\text{m}$, $T2 = 25 \mu\text{m}$, $R1 = 500 \mu\text{m}$, $R2 = 1000 \mu\text{m}$, $H = G1 = 15 \mu\text{m}$ for the segmented and continuous electrode devices when the pressure across the diaphragm is zero.

The CTE of Si is less than that of glass below about 100 °C. At this temperature, the integral part of (4) is maximal. Below this temperature, the relative coefficient of Si with respect to the glass is negative and it folds the response (Fig. 4). For the device with a segmented electrode, TCO is -13.3 ppm/K in the range of 25–50 °C, and 16.6 ppm/K in the range of 150–400 °C. For the device with a continuous skirt electrode, TCO is -15.4 ppm/K in the range of 25–50 °C, and 25.6 ppm/K in the range of 150–400 °C. It is clear that the former is less sensitive to temperature change. The reason is that when there is tensile residual stress in the device, the sidewall bends inwards, which is important in determining the electrode deflection. The stress in the continuous skirt electrode resists the sidewall deflection. For the device with a segmented skirt electrode, this stress is relieved making it less sensitive to residual strain.

F. Servo-Controlled Operation

The method employed for servo-controlled operation is to restore the sensing signal to its reference value. The diaphragm is not necessarily restored to its original undeflected position. This operation is shown in Fig. 5 and the parameters used are defined in Table I. When barometric pressure is applied, the diaphragm deflects, causing the deflection of the electrode, which, in turn, causes a capacitance change. Based on this capacitance change, the equivalent barometric force, F_d to the electrode can be calculated from the transfer function Z_d

$$F_d = Z_d P. \quad (5)$$

An electrostatic force, F_a , is applied by biasing the lower electrode to restore the capacitance. This is nonlinearly related to the applied voltage and capacitive gap. The total equivalent force applied on the electrode after feedback is

$$\Delta F = F_d - F_a. \quad (6)$$

As shown in Appendix I

$$F_a = Z_a \frac{Z_e A}{1 + Z_e Z_a A} Z_d P \quad (7)$$

where Z_e is capacitance change per unit pressure, Z_a is the electrostatic pressure per unit applied voltage, and A is the transfor-

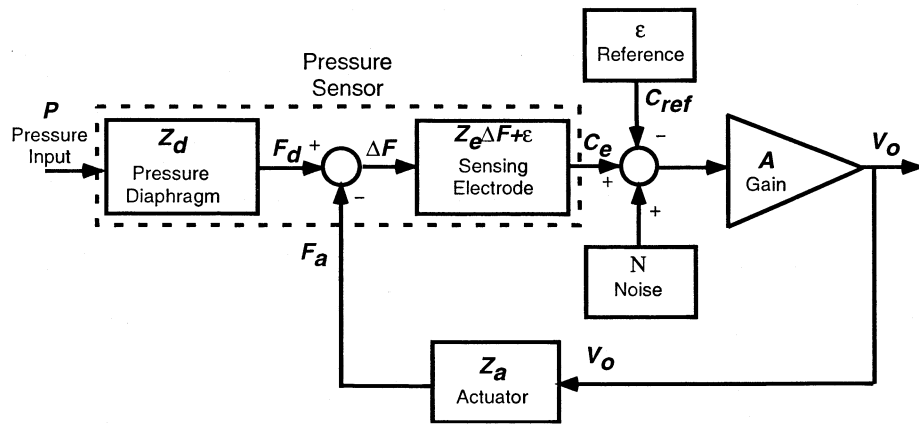


Fig. 5. Block-diagram for closed-loop operation.

 TABLE I
 DEFINITION OF THE VARIABLES USED IN FIG. 5

Variable	Physical Meaning
A [V/F]	Circuit gain from capacitance to voltage
C_e [F]	Capacitance output of pressure sensor
C_{ref} [F]	Reference capacitance
ϵ [F]	Capacitance offset at zero pressure
F_a [N]	Electrostatic force generated in feedback
F_d [N]	Mechanical force on sense electrode due to P
ΔF [N]	Net force on electrode
N [F]	Capacitance measurement uncertainty
P [N/m ²]	Barometric pressure
V_o [V]	Output voltage
Z_a [N/V]	Ratio of F_a to V_o
Z_d [m ²]	Ratio of F_d to P
Z_e [F/N]	Capacitance change per unit force on sense electrode

mation from capacitance to voltage. Thus, the net force applied on the diaphragm is

$$\Delta F = Z_d P - F_a = Z_d P - Z_a \frac{Z_e A}{1 + Z_e Z_a A} Z_d P. \quad (8)$$

As amplifier gain increases, the steady-state equivalent force on the diaphragm is zero

$$\Delta F \rightarrow 0 \quad \text{as} \quad Z_e A \rightarrow \infty. \quad (9)$$

The bias applied to the lower electrode also serves as the output signal

$$V_o = \frac{Z_e A}{1 + Z_e Z_a A} Z_d P \rightarrow \frac{Z_d}{Z_a} P \rightarrow \text{as } A \rightarrow \infty. \quad (10)$$

Coupled-field analysis is necessary to model this output voltage response of the pressure sensor, since both pressure and electrostatic forces must be simulated. Using MEMCAD software, a structure with dimensions $T1 = T2 = T3 = 10 \mu\text{m}$, $R1 = 500 \mu\text{m}$, $R2 = 1 \text{mm}$, $H = 10 \mu\text{m}$, and $G1 = 9 \mu\text{m}$, was meshed with a 10-node tetrahedral element. The dimensions of this device are well-suited to servo-controlled operation. The change in device capacitance with applied bias, which characterizes the feedback actuation, is plotted in Fig. 6 for

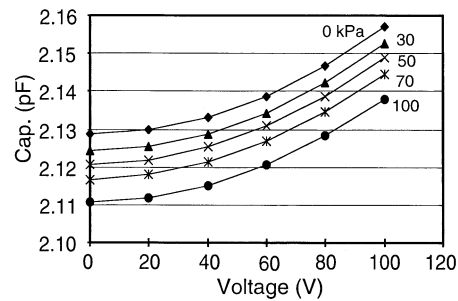


Fig. 6. Simulated feedback actuation over various pressures applied across the diaphragm.

various pressures across the diaphragm. The calculated pull-in voltage was $>100 \text{ V}$, the neutral capacitance was 2.13 pF , and the servo-controlled sensitivity was 0.64 V/kPa from 20 kPa to 90 kPa . The overall response is compared to measurements in Section IV.

G. Measurement Uncertainty and Noise

In Fig. 5, the measurement uncertainty or noise in the capacitance measurement is indicated by N , and the output voltage due to it is

$$\Delta V_o = \frac{A}{1 + Z_e Z_a A} N. \quad (11)$$

Dividing (10) by (11), it is evident that the resulting expression for signal to noise ratio is independent of the elements Z_a and A , which are related to the electrostatic feedback force. However, although servo-controlled operation does not change the nominal value of the signal to noise ratio of the transducer, it does help to reduce the uncertainty in the readout. In particular, (11) shows that for large A , the uncertainty is reduced by factor of $1/(Z_e Z_a)$. When a high dielectric constant liquid medium is used, Z_e and Z_a both increase. From another perspective, even though the sensitivity of the pressure sensor is nominally un-changed by the relative dielectric constant of the liquid ambient inside the package, the resolution—defined as $\Delta C_{\min}/(C \cdot S)$, where ΔC_{\min} is the minimum detectable capacitance change and S is the sensitivity—is increased by the dielectric constant of the medium.

H. Impact of Liquid Encapsulation: Dynamic Effects

Presence of liquid in the small sense gap causes the overall temporal response to be heavily overdamped, thereby reducing the susceptibility of the device to vibrations and transient accelerations. For a device with $T1 = T3 = 12 \mu\text{m}$, $T2 = 15 \mu\text{m}$, $R1 = 500 \mu\text{m}$, $R2 = 1000 \mu\text{m}$, and $H = 10 \mu\text{m}$, the natural frequency of the pressure sensor in air is 65 kHz, and the damping factor is about 0.23. However, the damping factor changes to 0.8 in the dielectric liquid, which has a viscosity of $1.313 \times 10^{-3} \text{N}\cdot\text{s}/\text{m}^2$.

III. FABRICATION & PACKAGING

A. Fabrication Sequence

The devices were fabricated by the three-mask dissolved wafer process. A Si wafer is first dry-etched to define the sidewall of the sealed cavity, then selectively diffused with boron to define the radius of the pressure sensor. To minimize the stress variation along the z-axis, postdiffusion annealing was performed at 1000°C for 20 min. The Si wafer was then flipped over and anodically bonded to a glass wafer that had been inlaid with a Ti–Pt–Au metal pattern that serves as interconnect and provides the bond pads. During anodic bonding, for some design variations, the out-diffusion of gas from the glass layer was blocked by a metal layer that was located within the cavity, although it was not used as an electrode. Since the encapsulated gas is mostly O_2 , the Ti layer in this metal film serve as a getter as well [13]. To increase yield, a dummy anchor surrounding the pressure sensor was devised. This dummy anchor delayed the exposure of the device sidewall to the etchant, and also increased the overall mechanical strength of the bond between the Si and glass wafers. The undoped Si was dissolved in a dopant-selective etchant. The lead transfer from the Si structure to the substrate occurred where the Si overlapped the metal inlaid on the glass. Since the cylinder has a narrow footprint, a protrusion was used to increase the alignment tolerance of the bond [5], [6]. A notch in the skirt electrode circumvents the additional rigidity due to this protrusion: fabricated devices are shown in Fig. 7.

B. Thermal Stress on Bonding Area

A point of interest in fabricating the device pertains to the shear force due to expansion mismatch between the glass and Si wafers. When it is assumed for simplicity that CTE of Si is independent of temperatures, the shear stress generated on the bonding surface is

$$\tau_{gs} = \frac{t_s^2}{T^2} \frac{(\alpha_g - \alpha_s)\Delta T}{\left(\frac{1-\nu_s}{E_s}t_s + \frac{1-\nu_g}{E_g}t_g\right)} \quad (12)$$

where ΔT is the difference between the bonding temperature and operating temperatures, α , E , ν , t_s , t_g , and T^2 denote the expansion coefficient, Young's modulus, Poisson ratio, thickness of the Si wafer, thickness of the glass wafer, and width of bonding area between silicon and glass. Since the bonded area in the device is only the footprint of the cavity sidewall, the shear force is sustained by a small area. This can lead to failure manifested as cracks in the glass as the wafers are cooled

after anodic bonding. However, it is evident from (12) that reducing the Si-wafer thickness relative to glass can alleviate this problem. It is convenient to chemically thin the Si wafer prior to bonding to release stress. Fig. 8 shows the estimated shear stress on bonding surface and normal stress across it as a function of the thickness of the Si wafer. These calculations assumed that $\alpha_s = 2.3 \text{ ppm}/\text{K}$, $\alpha_g = 1.3 \text{ ppm}/\text{K}$, $\Delta T = 300^\circ\text{C}$, $E_s = 160 \text{ GPa}$, $E_g = 73 \text{ GPa}$, $t_g = 600 \mu\text{m}$, $\nu = 0.23$ for both Si and glass and the w , width of bonding surface is $20 \mu\text{m}$. When the Si wafer was chemically thinned prior to bonding, the functional test yield for unpackaged devices was $>80\%$ with Corning Pyrex #7740 glass as a substrate.

C. Device Packaging

After fabrication, the wafers are diced and packaged. The package housing is composed of three parts: a steel cylinder, a thin stainless steel diaphragm and a brass base. The stainless steel diaphragm is welded to the cylinder. The motivation to use stainless steel is to prevent plastic deformation under high pressure. According to the ASME design code for flat-head pressure vessels [8]

$$t = d\sqrt{\frac{cP}{\sigma_m}} \quad (13)$$

where t is the minimum required thickness, d is a diameter of the stainless diaphragm, c is a numerical coefficient which depends on the method of attachment of diaphragm to cylinder, σ_m is maximum allowable stress, P is applied pressure and c is 0.5 for a circular plate welded to the end of a cylinder. This package can sustain 370 kPa, since the yield strength of the stainless steel is 2.1 GPa. The brass base provides six electric leads: four leads for wire bonding and two for electrical grounds for the package body. It has also has an open tube attached as shown in Fig. 9. The detailed dimensions of the package are provided in Table II.

Two pressure sensors were enclosed within each package. For the purpose of laboratory testing, the steel cylinder (along with the stainless steel diaphragm) was bonded to this brass bottom by using cyanoacrylate glue. A bulk polydimethylsiloxane (PDMS) plug, which had two small perforations, was inserted into the tube, and an inert liquid (Fluorinert-75) was injected through one perforation while the entrapped air bubbles were removed through the other perforation. Fluorinert is a chemically stable liquid and does not react with glue, and no swelling or shrinking of PDMS was observed due to it. To minimize the likelihood of a pressure increment induced by injection of fluid into the package, the package was left without sealing for 24 h. After this, a layer of cyanoacrylate glue was applied into the tube and the package was sealed fully.

Although the total volume of the inert liquid was 0.52 mL, this can be reduced along with the size of package as far as it does not affect the device performance. One criterion for the size is that the volume change in an empty package under applied pressure should be larger than volume change of the unpackaged pressure sensor under the same pressure, i.e., the compliance of the package must be greater than that of sensor. To estimate the volume change in package due to the deflection of the stainless steel diaphragm in the range upto 100 kPa, small deflection theory (bending deflection) is applicable. The estimated volume

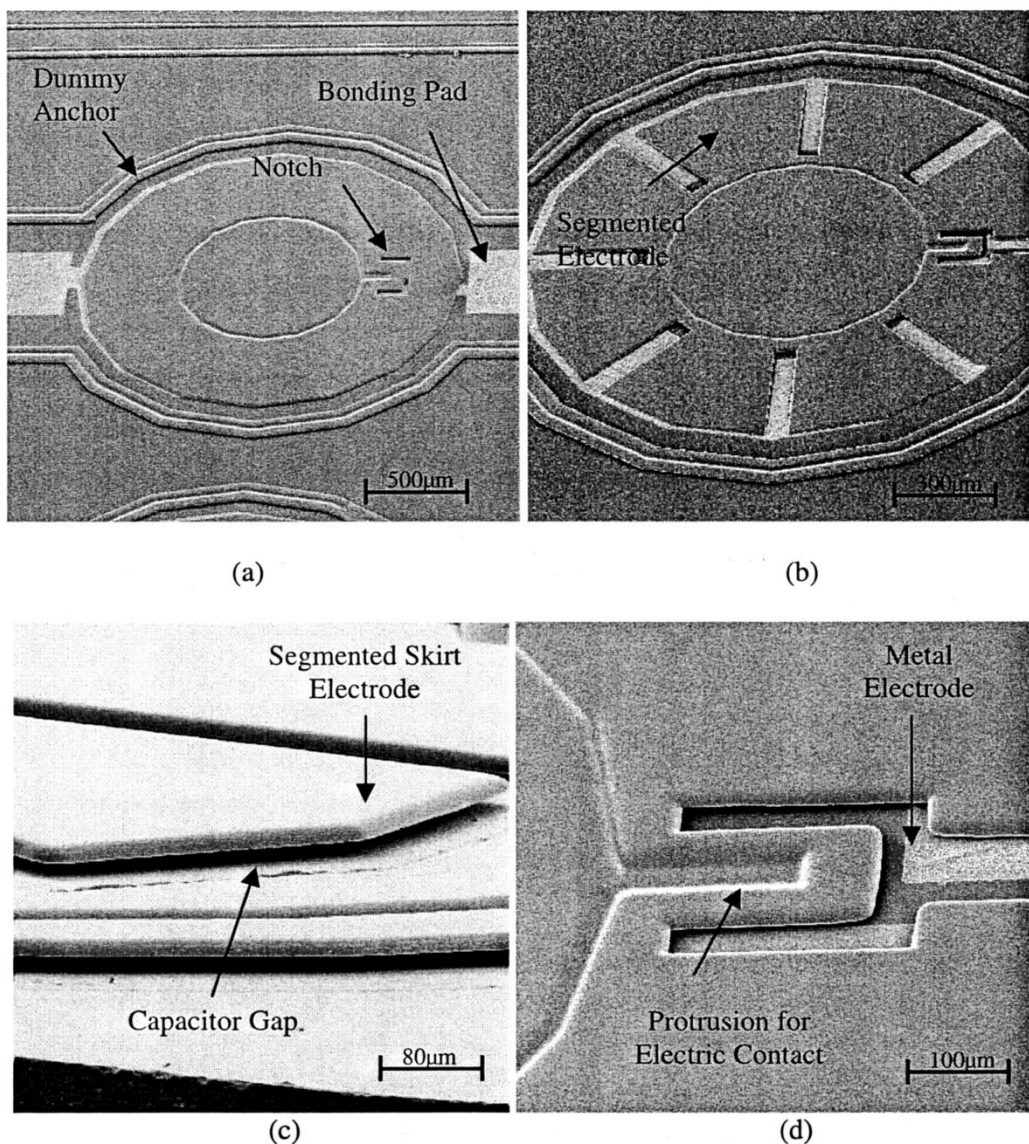


Fig. 7. SEM images of fabricated devices. (a) Device with continuous skirt electrode. (b) Device with segmented skirt electrode. (c) Gap between skirt electrode and substrate. The metal thin film on the substrate and the dummy anchor are also visible. (d) Protrusion of the sidewall for the lead transfer, and the associated notch in the skirt electrode.

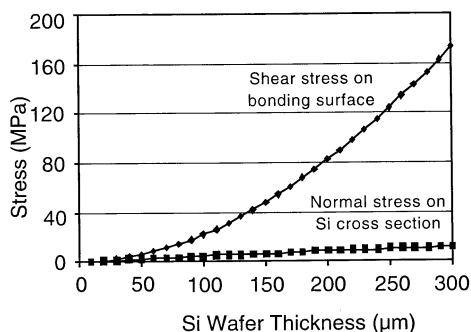


Fig. 8. Calculated shear stress at the bonding surface and normal stress in Si wafer.

package change is $4.89 \mu\text{L}$ at 100 kPa, while the volume change of the pressure sensor cavity is 1.82 nL at 100 kPa. The volume change of pressure sensor cavity is overestimated by small deflection theory. This suggests that the package does not limit the

device sensitivity. The package height can be reduced as long as the stainless steel diaphragm does not touch the Si diaphragm. The optical images of the device after packaging are shown in Fig. 10.

IV. EXPERIMENTAL RESULTS

Tests were performed on both unpackaged and packaged devices that were placed within a test chamber. *All measurements are referenced to the gauge pressure within the chamber*, which was measured by a Motorola MPX5100DP or Honeywell 40PC015G1A pressure sensor devices (upto 100 kPa). Above 100 kPa, a calibrated valve pressure gauge attached to gas tank served as the reference. The absolute pressure across the diaphragm calculated as explained below, is also noted on all measurements. The capacitance was measured by a Kiethley 590 CV Analyzer and HP 4284A Precision LCR meter. The results described in this section are typical and representative of each device type.

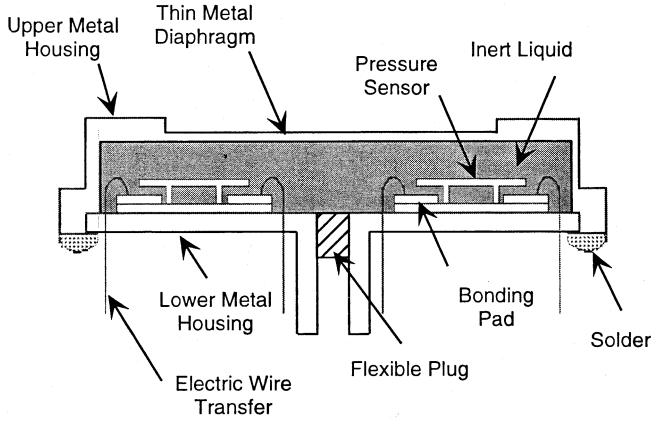


Fig. 9. The device is packaged in a liquid-filled metal housing with dimensions as described in Table II.

TABLE II
DIMENSIONS OF METAL PACKAGE ILLUSTRATED IN FIG. 9

Material	Dimension
Steel cap thickness	0.4 mm
Steel cap diameter	11.4 mm
Steel cap height	6.4 mm
Brass base thickness	0.5 mm
Diameter of port in base	3.28 mm
Stainless steel diaphragm thickness	75 μm
Stainless steel diaphragm diameter	~ 8 mm

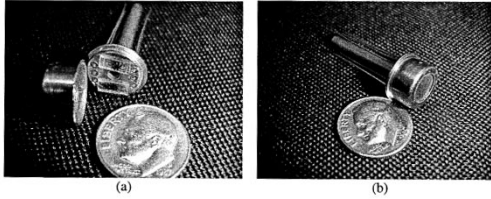


Fig. 10. Optical view of packaged device.

A. Cavity Pressure and Entrapped Gas

Due to equipment constraints, the cavity was sealed at atmospheric pressure at bonding temperatures of 400–550 °C. When anodic bonding is not done at low absolute pressure, gas is entrapped in the sealed cavity. The quantity of the gas depends on the anodic bonding temperature, and it changes the initial deflection state of pressure sensor at room temperature. As noted earlier, the structure for some devices included a metal thin film to block the gas which may out-diffuse from the glass substrate [13]. If it is assumed that the entrapped gas is only from the bonding conditions, the pressure across the diaphragm can be calculated using a few basic assumptions [14].

After anodic bonding and dissolution, as the device is returned to room temperature, the contraction of the gas causes a diaphragm deflection. At the equilibrium, the pressure in the cavity is

$$P_1 = \frac{mRT_1}{V_0 - \Delta V} \approx \frac{mRT_1}{V_0 - \frac{a^6(P_{\text{atm}} - P_1)\pi}{192D}} \quad (14)$$

where P is pressure, P_{atm} is the atmospheric pressure, V is volume of the vacuum cavity, m is entrapped air mass, R is universal gas constant for air (0.287 kN · m/kg · K), D is flexural

TABLE III
DEVICE DIMENSIONS AND MEASUREMENT RESULTS, WHICH ARE IN TERMS OF GAUGE PRESSURE. C_0 IS THE CAPACITANCE AT ZERO GAUGE PRESSURE. *LINEARITY FOR DEV1 WAS MEASURED OVER 0–250 kPa. FOR DEV2, DEV3, AND DEV4, LINEARITIES WERE MEASURED OVER 0–100 kPa

DEVICE	DEV1	DEV 2	DEV3	DEV 4 Segmented Skirt		
T1=T3 (μm)	9.7	12	12	12		
T2 (μm)	18	18	20	20		
H=G1 (μm)	10	15	15	15		
R1 (μm)	500	500	500	500		
R2 (μm)	1000	1000	1000	1000		
Bonding Temperature (°C)	550	350	450	450		
Unpackaged	Open Loop	C_0 (pF)	2.910	1.562	1.684	1.514
		Sensitivity (ppm/kPa)	-408	-154	-124	-136
		Sensitivity (fF/kPa)	-1.21	-0.24	-0.21	-0.21
	Closed Loop	Linearity (%)	<3.1	<4.5	<14.6	<6.5
		Sensitivity (V/kPa)	0.516	1.436	1.208	1.642
		Linearity* (%) (>20kPa)	<3.2	<2.6	<2.6	<1.8
Packaged	Open Loop	C_0 (pF)			2.882	2.646
		Sensitivity (ppm/kPa)			-137	-164
		$\Delta C/\Delta P$ (fF/kPa)			-0.39	-0.44
	Closed Loop	Linearity* (%)			<11.0	<4.7
		Sensitivity (V/kPa)			0.748	0.819
		Linearity (%) (>20kPa)			<1.4	<1.8

rigidity, T is absolute temperature, the subscript 0 indicates thermodynamic state at bonding, and subscript 1 indicates the thermodynamic state in the cavity at room temperature after the dissolution process. The volume change in the cavity after cooling down is ΔV

$$\Delta V = 2\pi \int_0^a r w(r) dr \approx 2\pi \int_0^a \frac{P_a - P_1}{64D} r (a^2 - r^2)^2 dr$$

$$= \frac{a^6(P_a - P_1)\pi}{192D} \quad (15)$$

where a is radius of the diaphragm, $w(r)$ is deflection of circular plate, and P_a is applied pressure on the circular diaphragm. To obtain this, it was assumed that the deflection is not large and axisymmetric bending theory can be applied. Also, the circular diaphragm was modeled with clamped edge boundary condition, which results in only $\sim 7\%$ discrepancy with ANSYS modeling for a typical device.

$$w(r) \approx \frac{P_a - P_1}{64D} (a^2 - r^2)^2 \quad (16)$$

The net pressure across the diaphragm can be estimated from (14) and (15).

Several devices with different dimensions were fabricated and tested as shown in Table III. DEV1 does not have a metal layer to block glass outgassing, unlike the rest of the devices listed. Thus, for all the remaining devices, using (14), the pressure across the diaphragm is 56.8 kPa for 0 kPa gauge pressure, and 153.1 kPa for 100 kPa gauge pressure.

B. Open Loop Measurements

Open-loop measurement response of DEV1 is shown in Fig. 11 with results for all devices summarized in Table III. The average sensitivity obtained by a least squares fit over the entire

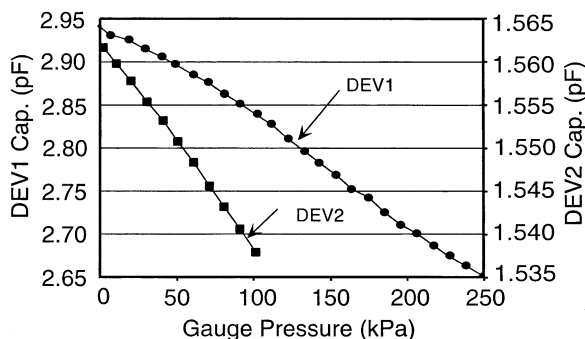


Fig. 11. Measured response in open-loop operation for DEV1.

tested range of 250 kPa is -408 ppm/kPa, with a reading of 2.91 pF at zero gauge pressure. While this sensitivity is lower than that of conventional capacitive pressure sensors, it does not pose a measurement challenge: capacitive accelerometers offer even smaller outputs, and commercial instrumentation can easily measure this. As noted earlier, the sensitivity can be increased by reducing the sense gap, e.g., by electroplating up the thickness of the metal electrode. Despite the wide dynamic range used in the test, no hysteresis was observed in the response, demonstrating that yield strength was not exceeded. It was also verified by FEA that for DEV1, the weakest device in Table III, the maximum von Mises stress, which occurs at the seam between the diaphragm and the sidewall is 369 MPa, well below the fracture limit of Si. The peak stress at the bonding interface to the substrate is only 177 MPa.

Measured results listed in Table III also show that the segmented skirt device (DEV4) achieves higher average sensitivity and better linearity (defined as the maximum variation from the best fit line, as a percentage of the full scale output) than DEV3, which is identical except that the skirt is not segmented. However, above 50 kPa gauge pressure, their sensitivities are similar.

C. Impact of the Stress Gradient

Variation in the stress along the z -axis in the boron-doped layer affects the flatness of the skirt [11], [15]. Although an annealing step is performed after boron diffusion to minimize this, a slight downward deflection at the free end of the skirt electrode exists. Based on design values, at zero gauge pressure the ratio of the capacitance (C_0) of DEV3 to DEV4 should be about 0.94 without considering fringing, because the segment cuts reduce the capacitor area. However, the measured ratio is 0.89 (see Table III). When the initial displacement is such that the skirt edge is lower than the cylinder height, the sensitivity is somewhat reduced because the bending moment from the residual stress, as explained in Section II, is reversed until the skirt is bending upward. As pressure is increased, the curvature in the skirt reverses, and with it, the sensitivity increases. Consequently, the pressure responses of DEV1 and DEV3 are bowed at low pressure, although this effect is minimized for DEV4 by the segmented electrode (see Fig. 12). In contrast to DEV3, DEV2 shows a very linear response to pressure. The ratio of C_0 between DEV2 and DEV4 is 0.98, which is higher than design value, because of the lower bonding temperature used for DEV2. Since this temperature was < 500 °C, the tensile stress

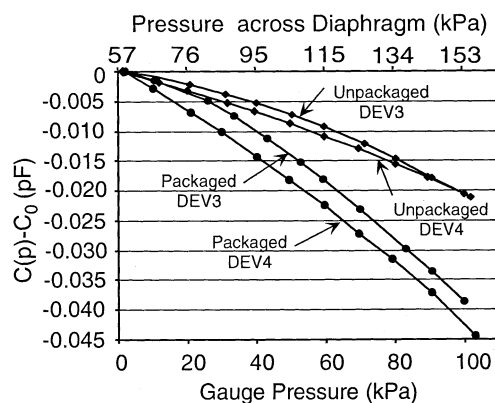


Fig. 12. Measured response of DEV3 and DEV4 in open-loop operation before and after packaging.

was greater, and resulted in a smaller C_0 . In addition, since the electrode is higher than the device height, DEV2 does not show a bowed response to pressure.

D. Impact of Liquid Encapsulation

After packaging DEV3 and DEV4, open-loop measurements were repeated. The dielectric constant of the inert liquid packaged inside package is theoretically 1.8. While packaged capacitance at zero pressure for each case was about 1.7 times of the unpackaged device, the sensitivity of packaged device was found to be 1.1–1.2 times larger than unpackaged devices. This is unexpected, because sensitivity is a fractional quantity. The reason may be that during packaging, the pressure in the package becomes higher than outside pressure, and it reduces C_0 .

E. Servo-Controlled Measurements

In preparation for servo-controlled measurements, the responses of the devices were characterized by measuring the capacitance change with applied bias at various pressures. Measurement results for packaged DEV3 and DEV4 are shown in Fig. 13. When the applied bias voltage was changed from 0 to 130 V at zero gauge pressure, the capacitance changes for DEV3 and DEV4 were 0.096 pF and 0.073 pF, respectively. The same trend was seen at other devices as well. This means DEV3 needs lower restoring voltage during servo-controlled operation (see Fig. 5). The reference capacitance is the capacitance at zero gauge pressure. However, if the reference capacitance is taken as the capacitance at zero pressure and a moderate bias voltage, then the operating voltage swing can be reduced.

Another interesting characterization is device response at different bias voltage levels. By applying voltage, the initial electrode deflection can be changed, and the device sensitivity to pressure can be tunable as a result. For DEV1, the open-loop sensitivity changes from -328 ppm/kPa to -437 ppm/kPa as the applied bias voltage is varied from 0 V to 65 V (see Fig. 14). The noise in this figure is due to a limitation of the equipment that was used for this particular measurement.

Servo-controlled operation of the pressure sensors was demonstrated by varying the chamber pressure and setting the bias voltage to provide the capacitance that was measured at

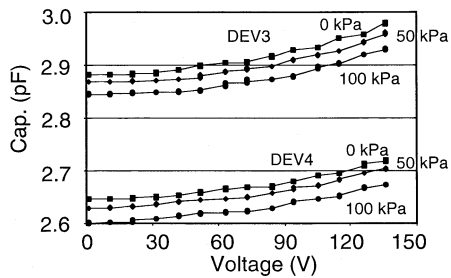


Fig. 13. Electrostatic deflection at various pressures for packaged devices DEV3 and DEV4, which has radial segments.

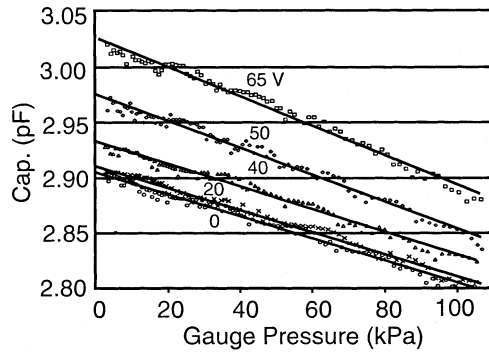


Fig. 14. Device response with various bias voltages for DEV1. Noise in this measurement is due to a low sense current that was limited by the apparatus.

zero gauge pressure. For the unpackaged DEV1 operating in air, the restoring voltage in servo-controlled operation was varied from 31.2–73.2 V as the pressure was varied from 20–100 kPa, providing an average sensitivity 0.516 V/kPa (Fig. 15). Over this range the response deviates from linearity by $\leq 3.22\%$ of the full-scale output. In addition to the measured results, Fig. 15 shows the output predicted by FEA. For gauge pressure lower than 60 kPa, the match is clearly very good. At larger pressures there is a deviation, possibly because the tetrahedral element that was used in FEA is structurally stiffer than the real value, and large deviation analysis was not accurate. Also, it is worth noting that the servo-controlled operation compensates nonlinear response as the cases for DEV2, DEV3, and DEV4 indicate (see Fig. 16).

For packaged devices DEV3 and DEV4, closed operation before and after packaging are compared in Fig. 16. In servo-controlled operation, the restoring voltages are affected by the dielectric constant of the inert liquid in package, which reduces the restoring voltages by factors of ≈ 1.8 for DEV3 and ≈ 1.7 for DEV4, respectively. These voltages can be further reduced by decreasing the sense gap as well.

In servo-controlled operation measurement results, it is clear that above 20 kPa pressure, the restoring voltage is almost linear with pressure (see Fig. 15 and 16). The change in slope at lower pressure can possibly be removed by biasing the electrode so that the structure is predeflected to the 20 kPa position. The entire dynamic range then causes the skirt electrode to deflect upward from this position.

F. Temperature Response

Reference devices designed to measure the TCO in a manner that eliminates the possibility of trapped gas were fabricated

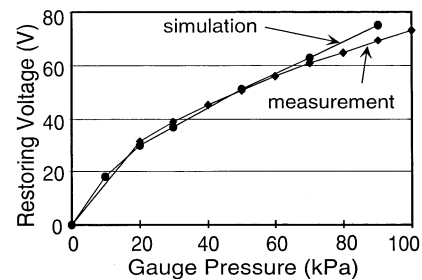


Fig. 15. Closed-loop response of the unpacked device, DEV1.

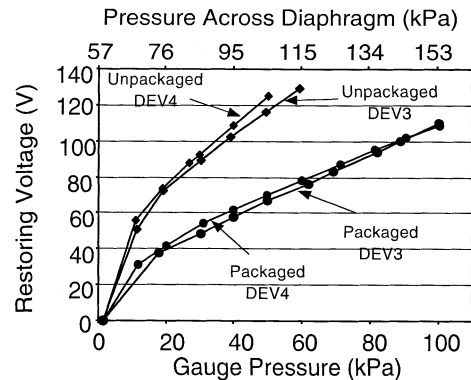


Fig. 16. Measured response of DEV3 and DEV4 in servo-controlled operation before and after packaging.

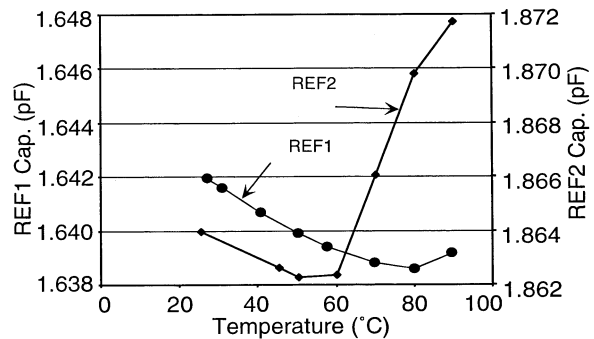


Fig. 17. Measured TCO of unpackaged devices REF1 and REF2 with $T_1 = T_3 = 12 \mu\text{m}$, $T_2 = 25 \mu\text{m}$, $H = 15 \mu\text{m}$, $R_1 = 500 \mu\text{m}$, and $R_2 = 1 \text{ mm}$. REF2 has a segmented electrode.

with small openings in the sidewalls. The differential pressure across the diaphragm is always zero for these devices. The reference device REF1 had the structural dimensions as $T_1 = T_3 = 12 \mu\text{m}$, $T_2 = 25 \mu\text{m}$, $H = 15 \mu\text{m}$, $R_1 = 500 \mu\text{m}$, and $R_2 = 1 \text{ mm}$. The reference device REF2 had the same dimensions, but had a segmented skirt electrode with 45° partitions. Both devices were on the same die. The devices were bonded at 450°C , but not packaged. The temperature response of these devices from room temperature upto 95°C is plotted in Fig. 17. Both devices clearly exhibit a negative TCO at low temperatures and positive TCO at the upper end of the tested range. For the device REF1, TCO is -38.2 ppm/K from 27°C to 80°C , and 36.5 ppm/K from 80°C to 90°C with respect to the capacitance at 27°C . Similarly, for the device REF2, TCO is -36 ppm/K from 25°C to 50°C , and 165 ppm/K from 60°C to 90°C . The reason that the TCO is folded around $50\text{--}80^\circ\text{C}$ is thermal expansion mismatch between single crystal Si (SCS)

and Pyrex #7740 glass. Thermal expansion curves of SCS and Pyrex #7740 cross around 100 °C and 500 °C [12]. The temperatures at which the TCO slope changes from negative to positive are around 60 °C and 80 °C for the two devices. These results match modeling results within 50 °C. Above 100 °C, TCO increases monotonically upto the bonding temperature. The measurements for a wider range were presented in [6].

The temperature coefficients for packaged devices were not measured. However, these are expected to be substantially worse than for the unpackaged devices because the volume expansion coefficient of the dielectric liquid used in the package is 1380 ppm/K and that of the brass housing is 19 ppm/K.

V. CONCLUSION

The results presented in Section IV demonstrate the open and servo-controlled operation of the pressure sensor, and their package. There are several points worth noting about the design and operation of this device.

First, for the dimensions that were selected, the closed-loop sensitivity was 0.516 V/kPa, which necessitated a 73.2-V bias for a dynamic range of 100 kPa. The bias can be reduced by increasing the diameter of the skirt or by reducing the capacitive gap between it and the electrode. As explained in [6], the gap may be reduced by increasing the thickness of the deposited metal that forms the electrode (e.g., by electroplating). Reducing the cavity height is not recommended because it reduces the overall compliance of the Si structure, and depending on the dimensions used, may result in lower sensitivity. Reducing the capacitive gap would increase the nonlinearity of the open-loop response.

Second, the sensitivity of the servo-controlled response can be electronically tuned. It was measured that a 100 kPa dynamic range requires a bias swing of 0–73 V if the reference capacitance is 2.91 pF. However, at 2.96 pF, the 0–100 kPa range requires a swing of only 53.9–82.3 V, which corresponds to a sensitivity of 0.284 V/kPa. This may be implemented, for example, by biasing the Si structure at –68 V and modulating the electrode voltage over a range of ±15 V. The advantage of this implementation is that standard electronics may be used for the servo-operation, while the bias supply, which is out of the loop, serves as a control parameter that could compensate for variations in manufacturing or operating conditions.

Third, the bias between the structure and electrode may also be used to tune the open-loop response. Fig. 14 shows that the average open-loop sensitivity over a 0–105 kPa dynamic range changes from –328 ppm/kPa to –437 ppm/kPa (a 33% increase) while the reference capacitance changes from 2.91 pF to 3.03 pF, as the bias increases from 0 to 65 V. (Note that the zero-bias sensitivity of –408 ppm/kPa obtained from Fig. 11 was averaged over a much wider dynamic range of 250 kPa.)

Fourth, by using high dielectric constant liquid as the medium that transmits pressure within the package, capacitive pick-off becomes easier, and restoring voltage for servo-controlled operation is reduced. The sensitivity depends on geometry, not on the dielectric constant. However, the capacitance change per unit pressure change increases linearly with dielectric constant of the medium. The dynamic range of the pressure sensor

was tested upto 250 kPa. Measurement noise for packaged device can be suppressed in servo-controlled operation. Both factors Z_a (electrostatic pressure/voltage) and Z_e (capacitance change/barometric pressure change), increase linearly with dielectric constant, so the measurement noise can be suppressed by the square of dielectric constant. Also, mechanical vibrations are damped by viscosity of the liquid. Consequently, the use of a dielectric liquid within the package is highly beneficial.

APPENDIX

With respect to Table I, in open-loop operation

$$C_e = Z_e \Delta F + \varepsilon \quad (\text{A.1})$$

$$V_o = A(C_e - C_{\text{ref}}) \quad (\text{A.2})$$

C_e can be provided by substituting (6) into (A.1)

$$C_e = Z_e(F_d - F_a) + \varepsilon. \quad (\text{A.3})$$

Substituting (A.3) into (A.2), V_o can be provided by

$$V_o = A[Z_e(F_d - F_a) + \varepsilon - C_{\text{ref}}] \quad (\text{A.4})$$

$$V_o = AZ_e(F_d - F_a) \quad \text{if } C_{\text{ref}} = \varepsilon. \quad (\text{A.5})$$

This signal is fed back to the electrostatic actuator, which generates force F_a :

$$F_a = Z_a V_o. \quad (\text{A.6})$$

Substituting (5) and (A.6) into (A.5), the output of the servo-controlled system is

$$V_o = AZ_e(Z_d P - Z_a V_o) \quad (\text{A.7})$$

$$V_o = \frac{Z_e A}{1 + Z_e Z_a A} Z_d P \quad (\text{A.8})$$

$$V_o = \frac{1}{Z_a} Z_d P \quad \text{as } Z_e A \rightarrow \infty. \quad (\text{A.9})$$

The electrostatic force can be obtained by substituting (A.8) into (A.6)

$$F_a = Z_a \frac{Z_e A}{1 + Z_e Z_a A} Z_d P. \quad (\text{A.10})$$

ACKNOWLEDGMENT

The authors gratefully acknowledge Prof. E. G. Lovell of University of Wisconsin-Madison for discussions.

REFERENCES

- [1] R. Puers, "Capacitive sensors: when and how to use them," *Sens. Actuators, Phys. A*, vol. 38, pp. 93–105, 1993.
- [2] A. V. Chavan and K. D. Wise, "A batch-processed vacuum-sealed capacitive pressure sensor," in *Proc. IEEE Int. Conf. on Solid-State Sensors and Actuators*, June 1997, pp. 1449–1452.
- [3] Y. Wang and M. Esashi, "A novel electrostatic servo capacitive vacuum sensor," in *Proc. IEEE Int. Conf. on Solid-State Sensors and Actuators*, June 1997, pp. 1457–1460.
- [4] B. P. Gogoi and C. H. Mastrangelo, "A low-voltage force-balanced pressure sensor with hermetically sealed servomechanism," in *Proc. IEEE Conf. on Microelectromechanical Systems*, Jan. 1999, pp. 493–498.
- [5] J.-S. Park and Y. B. Gianchandani, "A low-cost batch sealed capacitive pressure sensor," in *Proc. IEEE Conf. on Microelectromechanical Systems*, Jan. 1999, pp. 82–87.

- [6] —, "A capacitive absolute-pressure sensors with external pick-off electrodes," *J. Micromech. Microeng.*, vol. 10, pp. 528–533, 2000.
- [7] —, "A servo-controlled capacitive pressure sensor with a three mask fabrication sequences," in *Proc. IEEE Conf. on Solid State Sensors and Actuators (Transducers '01)*, 2001, pp. 506–509.
- [8] A. C. Ugural, *Stresses in Plates and Shell*. New York: McGraw-Hill, 1999.
- [9] R. D. Cook and W. C. Young, *Advanced Mechanics of Materials*. New York: Macmillan, 1985.
- [10] Y. B. Gianchandani and K. Najafi, "A bulk silicon dissolved wafer process for microelectromechanical devices," *J. Microelectromech. Syst.*, vol. 1, pp. 77–85, June 1992.
- [11] X. Ding, W. H. Ko, and J. M. Mansour, "Residual stress and mechanical properties of boron-doped p^+ silicon films," *Sens. Actuators*, vol. A21–A23, pp. 866–871, 1990.
- [12] W. H. Ko, J. T. Suminto, and G. J. Yeh, "Bonding techniques for microsensor," in *Micromachining and Micropackaging of Sensors*. New York: Elsevier Science, 1985.
- [13] Y. T. Cheng, W. T. Hsu, L. Lin, C. T. Nguyen, and K. Najafi, "Vacuum packaging technology using localized aluminum/silicon-to-glass bonding," *Proc. IEEE Microelectromechanical Systems*, pp. 18–21, Jan. 2001.
- [14] J.-S. Park, "Open Loop and Servo-Controlled Micromachined Capacitive Pressure Sensors," PhD Dissertation, Univ. Wisconsin-Madison, 2002.
- [15] Y. Zhang and K. Wise, "An ultra-sensitive capacitive pressure sensor with a bossed dielectric diaphragm," in *Dig. IEEE Solid-State Sensors and Actuators Workshop*, Hilton Head, SC, June 1994, pp. 205–208.
- [16] R. S. Muller *et al.*, Ed., *Microsensors*. New York: IEEE, 1990.



Jae-Sung Park received the B.S. and M.S. degrees in mechanical engineering from Postech and Seoul National University, Korea, in 1995 and 1997, respectively. He received Ph.D. degree in mechanical engineering from University of Wisconsin-Madison in 2002.

He is interested in design, fabrication, and testing of micromachined devices. Presently, he is working as a research fellow for bio-artificial liver in Harvard Medical School, and trying to bring MEMS technology to biological applications.



Yogesh B. Gianchandani (S'83–M'85) received the B.S., M.S., and Ph.D. degrees in electrical engineering from the University of California, Irvine, University of California, Los Angeles, and the University of Michigan, Ann Arbor, in 1984, 1986, and 1994, respectively.

He is presently with the Electrical Engineering and Computer Science Department at the University of Michigan. Prior to this, he was with the Electrical and Computer Engineering Department at the University of Wisconsin–Madison. He has also held industry positions with Xerox Corporation, Microchip Technology, and other companies, working in the area of integrated circuit design. His research interests include all aspects of design, fabrication, and packaging of micromachined sensors and actuators and their interface circuits.

Prof. Gianchandani received the National Science Foundation Career Award in 2000. He serves on the editorial boards of *Sensors and Actuators*, *IOP Journal of Micromechanics and Microengineering*, and *Journal of Semiconductor Technology and Science*. He also serves on the steering and technical program committees for the IEEE International Conference on Micro Electro Mechanical Systems (MEMS), and served as a General Co-Chair for this meeting in 2002.